

# Carbide precipitation in some secondary hardened steels

A. D. B. GINGELL, H. K. D. H. BHADESHIA

*Department of Materials Science and Metallurgy, Cambridge University, Pembroke street, Cambridge CB2 3Q2 UK*

D. G. JONES, K. J. A. MAWELLA

*Defence Research Agency, Fort Halstead Kent, TN 147 BP, UK*

The precipitation of alloy carbides in three commercial quenched and tempered martensitic steels has been studied using phase stability calculations, microscopy, microanalysis and dilatometry. The sequence of carbide stability as estimated using phase stability calculations is found to be consistent with the microstructural observations, if it is assumed that the equilibrium  $M_{23}C_6$  phase is suppressed by kinetic considerations. One interesting result is that the molybdenum-rich phase  $M_2C$  is neither predicted nor observed in any of the alloys, all of which contain substantial quantities of molybdenum. Other results include dilatometric experiments which enabled the measurement of transformation temperatures, which are compared against theoretical values.

## 1. Introduction

Martensitic steels usually have to be tempered in order to obtain an optimum combination of strength and toughness. The tempering process usually leads to a decrease in strength due to the precipitation of iron carbides from carbon that was originally in solid solution in the martensite. However, when the steel contains strong carbide-forming elements such as molybdenum, vanadium and chromium, it becomes possible to recover the strength during prolonged tempering at elevated temperatures. This is called secondary hardening – it occurs because substitutional alloying elements (such as Cr) can diffuse during prolonged annealing to precipitate finely dispersed alloy carbides (see for example, reference [1]).

The alloy carbides found in secondary-hardened steels are thermodynamically more stable than iron carbides and show little tendency to coarsen. However, many of the alloy carbides find it difficult to nucleate, so that the equilibrium carbide is not necessarily the first to precipitate. Instead, there is a sequence of alloy carbides precipitated in an order determined by a combination of kinetic and thermodynamic considerations, but which leads ultimately towards an equilibrium microstructure. The aim of the present work was to investigate the precipitation of alloy carbides during the tempering of three high strength secondary hardened steels with slightly different chemical compositions. The steels are a part of a programme of research aimed at the optimization of strength and toughness.

## 2. Experimental procedures

### 2.1. Material

The three steels investigated were provided by the Defence Research Agency, Fort Halstead. They were

supplied in standard (steel 1), high purity (steel 2) and modified high purity (steel 3) forms. Their compositions are given in Table I.

Steel 1 is a conventional secondary hardening alloy produced commercially, with deliberate additions of manganese and silicon. These elements have little effect on the secondary hardening but are known to embrittle steels through segregation to the austenite grain boundaries [2]. Consequently their removal should improve toughness. Steel 2 is a high purity steel with a similar composition to steel 1 but with manganese and silicon removed. Finally, steel 3 is also a high purity steel but with a higher concentration of carbon and alloying elements to give a greater fraction of carbides in the final microstructure.

### 2.2. Thermodynamic modelling

Equilibrium phase diagram calculations were carried out using MTDATA [3], taking into account the following components and phases (the  $M$  in each of the carbide phases refers to metal atoms, and the  $a$  represents ferrite):

System components: Fe, C, Mn, Si, Mo, V, Ni, Cr  
 System phases: ferrite,  $M_2C$ ,  $M_3C$ ,  $M_7C_3$ ,  $M_{23}C_6$ ,  $M_6C$

The calculations were conducted for a temperature of 560 °C, corresponding to the tempering temperature used commercially. The sequence of thermodynamic stability can be examined by first conducting the calculations with all phases permitted. The suppression from the calculation of the carbide phase which is found to be dominant then allows the next most stable phase to appear, so that a sequence of carbide

TABLE I Chemical compositions of the steels (wt %)

	C	S	P	Si	Mn	Ni	Cr	Mo	V
Steel 1	0.33	0.003	< 0.002	0.24	0.44	3.33	0.93	0.65	0.20
Steel 2	0.31	0.002	0.003	0.03	0.01	3.56	0.98	0.96	0.18
Steel 3	0.38	0.002	< 0.01	< 0.05	< 0.03	3.65	1.23	1.54	0.21

precipitation based on thermodynamic stability can be determined.

### 2.3. Microscopy

Thin foil transmission electron microscopy (TEM) was carried out to characterize the actual microstructures that develop on tempering. The three alloys were austenized at 870 °C for 2 h, water quenched to room temperature and tempered at 560 °C for varying lengths of time, in the range of 1–16 h. All heat treatments were carried out with the samples sealed in evacuated silica tubes in order to prevent oxidation and decarburization of the steels. The microscopy was performed using a Philips 400 TEM operating at 120 kV using bright field and dark field imaging and selected area diffraction patterns to identify the carbides. Microanalysis has also been used to confirm the substitutional solute content of the carbides.

### 2.4. Dilatometry

Austenite formation begins during heating at the  $A_{c1}$  temperature and is completed when the  $A_{c3}$  temperature is reached. The latter temperature naturally defines the lower limit of the austenization temperature. Tempering must be carried out below the  $A_{c1}$  temperature because the partial formation of austenite during tempering would lead to the formation of brittle untempered martensite on cooling. The austenite formation temperatures were therefore determined using dilatometry and compared with theoretical estimates based on the alloy composition. The experiments also allowed a direct measurement of the martensite-start temperatures during cooling from the austenitic state. These were compared against calculated values.

The dilatometry was carried out using a “Thermecmaster” thermomechanical simulator. Cylindrical specimens 12 mm in height and 8 mm in diameter were heated at rates in the range 1–20 °C s<sup>-1</sup> to 1200 °C and quenched at 10 °C s<sup>-1</sup>. Phase transformations were detected by monitoring the fractional change in dilatation with temperature.

## 3. Results

### 3.1. Phase stability calculations

The phase diagram calculations revealed significant differences between the three alloys. The most dominant equilibrium carbide was in all cases found to be  $M_{23}C_6$ . This was the sole alloy carbide for steel 3, whereas  $M_2C$  and  $M_3C + M_7C_3$  could coexist with  $M_{23}C_6$  in steels 2 and 1 respectively. The mole per cent of each phase, along with the partition of the alloying

elements in each phase, is given for the three steels in Tables II–IV

The  $M_{23}C_6$  carbide is therefore the most dominant precipitate under equilibrium conditions, but is unlikely to form immediately at 560 °C due to a large activation energy for nucleation. It generally forms through a precipitation sequence involving  $M_3C$  and  $M_7C_3$  [4]. In the meantime, other carbides can precipitate and the identity of these carbides can sometimes be revealed by suppressing the  $M_{23}C_6$  phase in the calculations to give the next most thermodynamically stable carbide. Tables V–VII give the results of the calculations for each steel at 560 °C for the case where  $M_{23}C_6$  is suppressed. The calculations were also carried out over a temperature range of 500–700 °C, typical of that used for the tempering of high strength steels; those results are illustrated in Figs 1–3.

It can be seen that in the absence of  $M_{23}C_6$ , the main carbides that form are  $M_3C$  and  $M_7C_3$ , with some  $M_6C$  in the more heavily alloyed steels 2 and 3. Of particular interest is the higher chromium and molybdenum concentrations in  $M_7C_3$  compared to  $M_3C$ , and the very high molybdenum concentration in  $M_6C$ . Examination of the variation of carbide concentration with temperature (Figs 1–3) reveals an increase in the mole fraction of  $M_3C$  with increasing tempering temperature, at the expense of the  $M_7C_3$  carbide. Steels 2 and 3 would be expected to contain some  $M_6C$  which is absent from steel 1, and both steel 1 and steel 2 have temperatures at which  $M_2C$  is stable at the expense of  $M_7C_3$ , both carbides being molybdenum-rich. In all three steels the relative amounts of carbides are similar, but the striking difference is in the total carbide content, which is significantly higher in steel 3. This accounts immediately for the higher hardness of steel 3 after tempering (Fig. 4).

### 3.2. Microscopy

Transmission electron microscopy showed the microstructures of all three alloys to be similar, with little change in carbide size and distribution during tempering in the range 1–16 h. Selected area diffraction patterns confirmed the presence of  $M_3C$  and  $M_7C_3$  carbides. Larger  $M_{23}C_6$  particles were also identified, and diffraction studies indicated the presence of some  $M_6C$ , although this could not be identified unambiguously. The  $M_2C$  carbide was never positively identified using electron microscopy.

The carbides were found to adopt distinctive morphologies.  $M_3C$  (orthorhombic,  $a = 0.45241$  nm,  $b = 0.50883$  nm,  $c = 0.67416$  nm) occurred as elongated carbide plates aligned along  $\langle 111 \rangle$  matrix

TABLE II Composition and mole percentage of equilibrium carbides in steel 1 at 560 °C

Phase	Mole percentage	Composition (mole fraction)							
		Fe	Cr	Mn	Ni	Mo	V	Si	C
Ferrite	93.5	0.955	0.001	0.002	0.033	–	0.002	0.005	–
M <sub>3</sub> C	1.3	0.600	0.075	0.064	0.011	–	–	–	0.250
M <sub>7</sub> C <sub>3</sub>	1.1	0.270	0.313	0.113	–	0.004	–	–	0.300
M <sub>23</sub> C <sub>6</sub>	4.1	0.605	0.099	–	–	0.090	–	–	0.207

TABLE III Composition and mole percentage of equilibrium carbides in steel 2 at 560 °C

Phase	Mole percentage	Composition (mole fraction)							
		Fe	Cr	Mn	Ni	Mo	V	Si	C
Ferrite	93.5	0.961	0.002	–	0.036	–	–	0.001	–
M <sub>2</sub> C	0.6	0.002	0.326	0.002	–	0.044	0.292	–	0.333
M <sub>23</sub> C <sub>6</sub>	5.9	0.589	0.115	–	–	0.090	–	–	0.207

TABLE IV Composition and mole percentage of equilibrium carbides in steel 3 at 560 °C

Phase	Mole percentage	Composition (mole fraction)							
		Fe	Cr	Mn	Ni	Mo	V	Si	C
Ferrite	91.5	0.956	0.002	–	0.038	–	0.003	0.001	–
M <sub>23</sub> C <sub>6</sub>	8.5	0.559	0.131	–	–	0.103	–	–	0.207

TABLE V Composition and mole percentage of equilibrium carbides in steel 1 at 560 °C, in the absence of M<sub>23</sub>C<sub>6</sub>

Phase	Mole percentage	Composition (mole fraction)							
		Fe	Cr	Mn	Ni	Mo	V	Si	C
Ferrite	94.6	0.957	0.001	0.001	0.033	–	0.002	0.005	–
M <sub>3</sub> C	1.9	0.643	0.058	0.034	0.010	0.004	–	–	0.250
M <sub>7</sub> C <sub>3</sub>	3.5	0.302	0.223	0.074	–	0.101	–	–	0.300

TABLE VI Composition and mole percentage of equilibrium carbides in steel 3 at 560 °C, in the absence of M<sub>23</sub>C<sub>6</sub>

Phase	Mole percentage	Composition (mole fraction)							
		Fe	Cr	Mn	Ni	Mo	V	Si	C
Ferrite	94.7	0.960	0.001	–	0.035	–	0.002	0.001	–
M <sub>3</sub> C	2.0	0.668	0.066	0.001	0.010	0.005	–	–	0.250
M <sub>7</sub> C <sub>3</sub>	2.9	0.313	0.272	0.002	–	0.113	–	–	0.300
M <sub>6</sub> C	0.4	0.338	0.007	–	–	0.512	–	–	0.143

TABLE VII Composition and mole percentage of equilibrium carbides in steel 3 at 560 °C, in the absence of M<sub>23</sub>C<sub>6</sub>

Phase	Mole percentage	Composition (mole fraction)							
		Fe	Cr	Mn	Ni	Mo	V	Si	C
Ferrite	93.5	0.958	0.001	–	0.037	–	0.002	0.001	–
M <sub>3</sub> C	1.7	0.667	0.066	0.002	0.011	0.005	–	–	0.25
M <sub>7</sub> C <sub>3</sub>	4.0	0.313	0.267	0.005	–	0.115	–	–	0.300
M <sub>6</sub> C	0.8	0.338	0.007	–	–	0.512	–	–	0.143

directions, giving Widmanstätten-type arrays (Fig. 5). M<sub>7</sub>C<sub>3</sub> (trigonal,  $a = 1.3982$  nm,  $c = 0.4506$  nm) was present on a finer scale with a more rounded shape than the M<sub>3</sub>C carbide (Fig. 6). The M<sub>7</sub>C<sub>3</sub> carbide

contained stacking faults along  $\{10\bar{1}0\}$  planes, giving easily identifiable streaks on diffraction patterns. These streaks were not easily observed during thin foil transmission electron microscopy because of strong

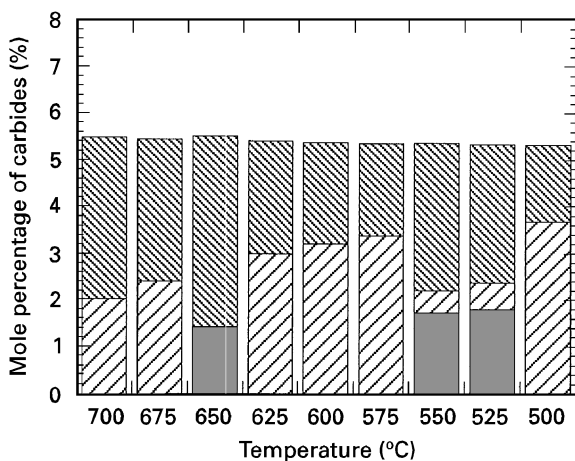


Figure 1 Mole percentage of carbides in Steel 1 in the absence of  $M_{23}C_6$ . Key: (■)  $M_3C$ , (▨)  $M_7C_3$  and (■)  $M_2C$ .

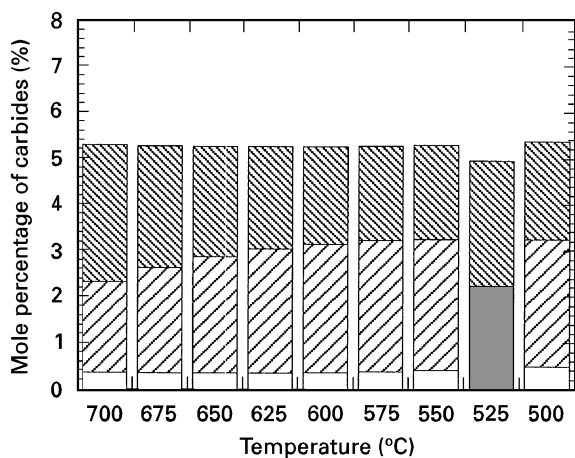


Figure 2 Mole percentage of carbides in steel 2 in the absence of  $M_{23}C_6$ . Key: (■)  $M_3C$ , (▨)  $M_7C_3$ , (■)  $M_2C$  and (□)  $M_6C$ .

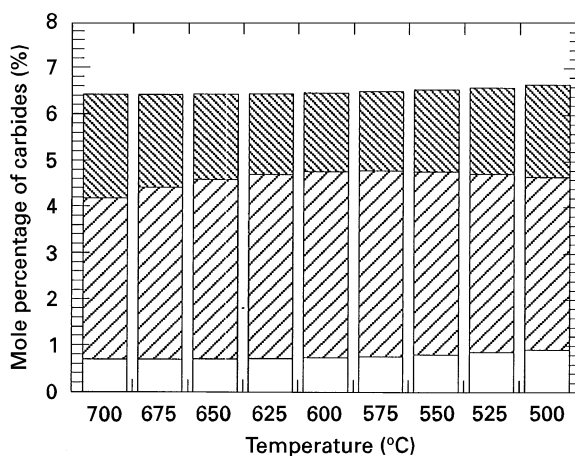


Figure 3 Mole percentage of carbides in Steel 3 in the absence of  $M_{23}C_6$ . Key: (■)  $M_3C$ , (▨)  $M_7C_3$  and (□)  $M_6C$ .

diffraction from the matrix, but were readily visible in carbon extraction replica samples, where there is no background diffraction to mask the contributions from particles. All three steels also contain larger particles, typically on lath boundaries (Fig. 7), which could be either  $M_{23}C_6$  or  $M_6C$ , both carbides having

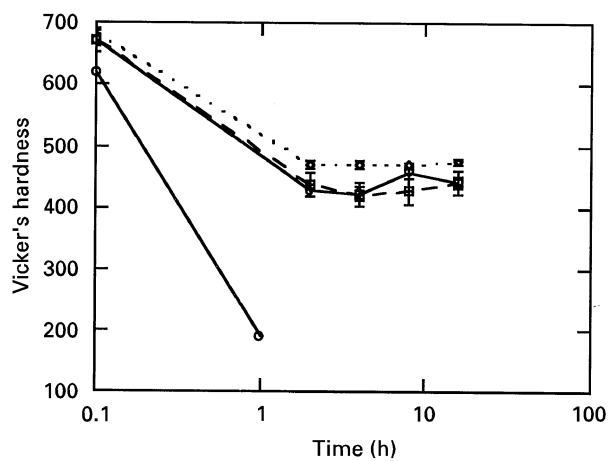


Figure 4 Variation of hardness ( $kg\ mm^{-2}$ ) with tempering time at  $560\ ^\circ C$ . Key: (○) Fe-0.35 wt %C, (●) Steel 1, (□) Steel 2 and (△) Steel 3.

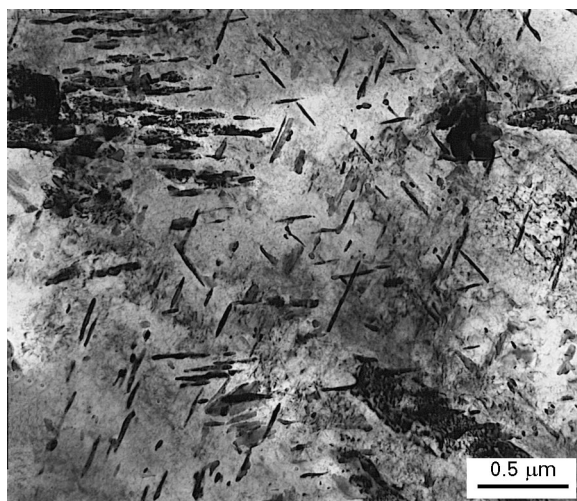


Figure 5  $M_3C$  carbides in steel 2, after tempering for 2 h at  $560\ ^\circ C$ .

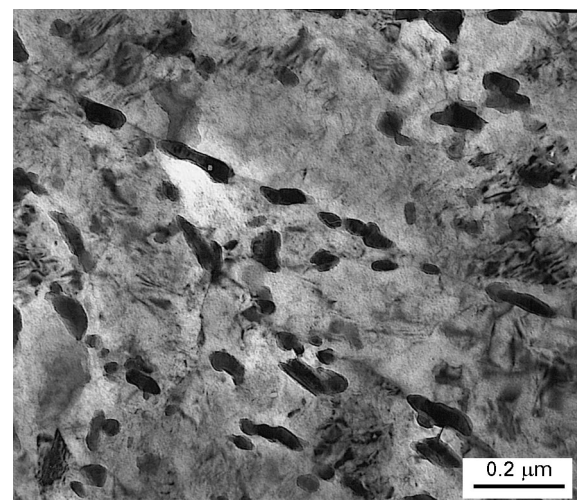


Figure 6  $M_7C_3$  carbides in steel 2, tempered for 16 h at  $560\ ^\circ C$ .

face-centred cubic structures with similar unit cell parameters (1.0638 nm and 1.1082 nm respectively). As stated above,  $M_2C$  (hexagonal,  $a = 0.3002\ nm$ ,  $c = 0.4506\ nm$ ) was never positively identified using

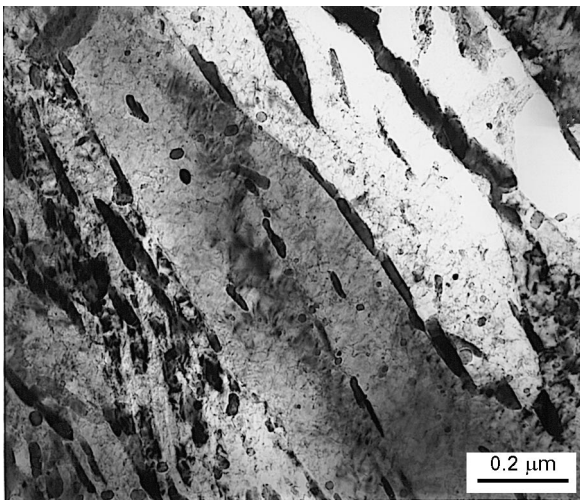


Figure 7 Lath boundary carbides in steel 2, tempered for 2 h at 560 °C.

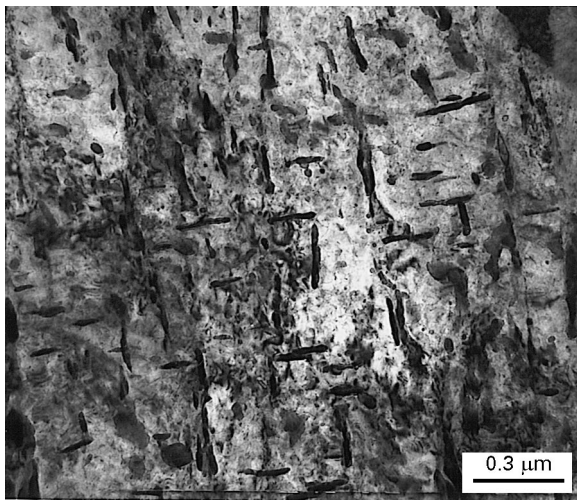


Figure 8 Orthogonal carbides in steel 2, tempered for 16 h at 560 °C.

electron diffraction. This carbide usually forms as needles aligned with  $\langle 100 \rangle$  directions, giving a distinctive perpendicular array of fine carbides. Although not extensive, such an array has been observed in steel 2 (Fig. 8) but it is not representative of the main carbide form.

Microanalysis of the carbides was carried out using energy dispersive X-ray analysis (EDX) on carbon extraction replicas of steel 1 tempered for 2 h. Preliminary results suggest that both rounded and aligned particles appear to have similar compositions, with chromium contents in the range 3–6 wt % and molybdenum contents in the range 4–20 wt %, with molybdenum consistently having a greater concentration than chromium. These compositions discount  $M_2C$ , which has a significant vanadium content,  $M_3C$ , which contains very little molybdenum, and  $M_6C$ , which contains very high levels of molybdenum (Tables II–IV). It is unlikely that  $M_{23}C_6$  forms after 2 h of tempering so the carbides are most probably  $M_7C_3$ , as suggested by the diffraction studies. This carbide usually has a much higher chromium content (see Table II) but after only 2 h of tempering the

equilibrium solute concentrations within carbides are unlikely to have developed.

### 3.3. Transformation temperatures

The austenite start and finish temperatures,  $Ac_1$  and  $Ac_3$ , and the martensite start temperature,  $M_s$ , were determined experimentally using a “ThermecMastor” thermomechanical simulator. The variation in specimen dimensions with temperature during both heating and cooling is shown in Fig. 9. The transformation temperatures are defined as the points where the curve leaves the tangent to the linear portion. The variation in  $Ac_1$  and  $Ac_3$  with heating rate for the three steels is given in Table VIII. In all cases the transformation temperatures are highest for steel 3 and lowest for steel 1, reflecting the higher alloy content of steel 3. The  $Ac_3$  temperature is more sensitive to both composition (steel type) and heating rate than the  $Ac_1$  temperature, which notably shows no dependence on heating rate for 10 and 20 °C s<sup>-1</sup> in all three steels.

The martensite start temperature for each steel, determined using a quench rate of 10 °C s<sup>-1</sup>, is given in Table IX, along with theoretical values determined

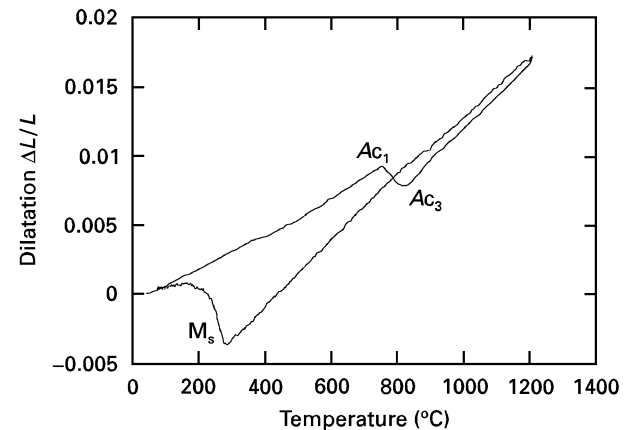


Figure 9 Actual dilatation variation with temperature on heating and cooling between room temperature and 1200 °C, in steel 1 heating at 20 °C s<sup>-1</sup> and cooling at 10 °C s<sup>-1</sup>.

TABLE VIII Start and finish temperature for the ferrite–austenite transformation on heating

Heating rate (°C s <sup>-1</sup> )	Steel 1		Steel 2		Steel 3	
	$Ac_1$ (°C)	$Ac_3$ (°C)	$Ac_1$ (°C)	$Ac_3$ (°C)	$Ac_1$ (°C)	$Ac_3$ (°C)
1	724	776	734	778	737	786
10	752	806	766	819	769	833
20	752	823	763	840	769	847

TABLE IX Theoretical and experimental values for the martensite start temperature (°C)

	Steel 1	Steel 2	Steel 3
Theoretical	300	321	268
Experimental	290 ± 5	310 ± 10	275 ± 10

from calculations of the time–temperature-transformation (TTT) diagram based on the alloy composition [5]. Steel 3, with its higher carbon and alloy content, has a significantly lower  $M_s$  temperature than the other two steels. Steel 2, with the lowest carbon content, has the highest  $M_s$  temperature. In all three cases there is good agreement between theoretical and experimental values.

#### 4. Discussion

It is evident that the tempering heat treatments used do not lead to the formation of the thermodynamically most stable carbide,  $M_{23}C_6$ , which forms as relatively coarse particles. However, finer intermediate carbides can precipitate during tempering, and for maximum strengthening effect it is important to obtain the optimum distribution of alloy carbides. In Cr–Mo–V steels the greatest strengthening effect has been attributed to molybdenum and vanadium-rich  $M_2C$  carbides forming in sheets of needles along  $\langle 100 \rangle$  ferrite directions, with  $M_7C_3$  and  $M_3C$  having lesser strengthening effects [6]. However it is apparent both from thermodynamic modelling and transmission electron microscopy that for the alloy chemistries of the steels used in this study that the secondary hardening strengthening effect is due to the precipitation of  $M_7C_3$  and  $M_3C$  non-equilibrium carbides, and not to the precipitation of  $M_2C$ . Consequently the difference in strength levels between steel 3 and the other two steels is due to the greater mole fraction of carbides through its higher carbon and alloy concentration, and not to any difference in precipitation sequence as was originally suspected.

The dilatometry experiments provide important information for the heat treatment of these alloys. In all cases the austenite start temperature is above  $700^\circ\text{C}$ , which is considered the upper limit for tempering heat treatments. The development of austenite during tempering would alter the microstructure and have deleterious effects upon the mechanical properties of tempered steels. The austenite finish temperature reaches its maximum at  $847^\circ\text{C}$  in steel 3, which again defines a limit for the austenization temperature of these steels. Above  $900^\circ\text{C}$ , the grain boundary pinning particles  $V_4C_3$  start to dissolve, leading to austenite grain growth and subsequent deleterious effects on mechanical properties. Therefore austenization is best carried out in the range  $850\text{--}900^\circ\text{C}$ . The good agreement between experimental and theoretical martensite start temperatures is encouraging, and future work will consider the sensitivity of martensite and bainite

formation to cooling rate, which is of importance in the quenching and tempering of large sections where cooling rates are non-uniform across the section.

#### 5. Conclusions

Thermodynamic modelling predicts the formation of  $M_{23}C_6$  as the most stable carbide during tempering of three Cr–Mo–V steels at  $560^\circ\text{C}$ . It also predicts the precipitation of  $M_7C_3$  and  $M_3C$  as the principal non-equilibrium carbides.  $M_2C$  is not predicted at  $560^\circ\text{C}$ , although it is stable at various temperatures in the range  $500\text{--}700^\circ\text{C}$  for steels 1 and 2. Thin foil transmission electron microscopy confirms the findings of the thermodynamic modelling with a fine distribution of  $M_7C_3$  and Widmanstätten arrays of  $M_3C$ . There is little difference in the carbide distributions of the three steels, and the greater secondary hardening response of steel 3 is accounted for by its higher carbon and alloy content giving a greater mole fraction of carbides. Microanalysis of  $M_7C_3$  carbides after 2 h of tempering suggests that carbide composition is non-equilibrium. Dilatometry has confirmed the austenite and martensite transformation temperatures, the latter agreeing with theoretical values. These values give safe limits for suitable secondary heat treatments.

#### Acknowledgements

This paper describes work supported by the Defence Research Agency, Fort Halstead, Kent. The authors would like to thank Professor C.J. Humphreys for the provision of research facilities.

#### References

1. R. W. K. HONEYCOMBE and H. K. D. H. BHADSHIA, "Steels: microstructure and properties", 2nd Edn. (Edward Arnold, London, 1995).
2. C. J. McMAHON, Jr., in "Innovations in ultrahigh-strength steel technology", edited by G. B. Olson, M. Azrin and E. S. Wright (US Army Materials Laboratory Command, New York, 1987) pp. 597–618.
3. F. B. PICKERING, "Physical metallurgy and the design of steels", (Applied Science Publishers, Barking, UK, 1978) p. 133.
4. "MTDATA – metallurgical and thermochemical data", (National Physical Laboratory, Teddington, UK 1994).
5. H. K. D. H. BHADSHIA, *Metal Sci.* **15** (1981) 178.
6. R. G. BAKER and J. NUTTING, *J.I.S.I.* **192** (1959) 257.

Received 11 July 1996  
and accepted 7 April 1997